Epithelial polarity requires septin coupling of vesicle transport to polyglutamylated microtubules

Elias T. Spiliotis,[1] Stephen J. Hunt,[1] Qicong Hu,[1] Makoto Kinoshita,[2] and W. James Nelson[1]

[1]Departments of Biology, and Molecular and Cellular Physiology, Stanford University, Stanford, CA 94305
[2]Biochemistry and Cell Biology Unit, HMRO, Kyoto University, Kyoto 606-8501, Japan

In epithelial cells, polarized growth and maintenance of apical and basolateral plasma membrane domains depend on protein sorting from the trans-Golgi network (TGN) and vesicle delivery to the plasma membrane. Septins are filamentous GTPases required for polarized membrane growth in budding yeast, but whether they function in epithelial polarity is unknown. Here, we show that in epithelial cells septin 2 (SEPT2) fibers colocalize with a subset of microtubule tracks composed of polyglutamylated (polyGlu) tubulin, and that vesicles containing apical or basolateral proteins exit the TGN along these SEPT2/polyGlu microtubule tracks. Tubulin-associated SEPT2 facilitates vesicle transport by maintaining polyGlu microtubule tracks and impeding tubulin binding of microtubule-associated protein 4 (MAP4). Significantly, this regulatory step is required for polarized, columnar-shaped epithelia biogenesis; upon SEPT2 depletion, cells become short and fibroblast-shaped due to intracellular accumulation of apical and basolateral membrane proteins, and loss of vertically oriented polyGlu microtubules. We suggest that septin coupling of the microtubule cytoskeleton to post-Golgi vesicle transport is required for the morphogenesis of polarized epithelia.

Introduction

The plasma membrane of polarized columnar-shaped epithelial cells is segregated into functionally distinct apical and basolateral domains that face different biological compartments and regulate vectorial transport of ions and solutes. Biogenesis of these membrane domains and maintenance of cell shape depend on protein sorting during vesicle budding from the TGN and endosomes, transport of vesicles along the actin and microtubule cytoskeleton, and their fusion with the appropriate membrane domain (Griffiths and Simons, 1986; Matter and Mellman, 1994; Mostov et al., 2000; Rodriguez-Boulan et al., 2005).

The microtubule cytoskeleton is involved in long-range transport of vesicular carriers and in the morphogenesis of columnar-shaped, polarized epithelial cells (Musch, 2004). During polarization, microtubules are organized into a vertical network that orients along the apicobasal cell axis (Musch, 2004; Rodriguez-Boulan et al., 2005). TGN-derived vesicular carriers associate with microtubules (Van der Sluijs et al., 1990; Hirschberg et al., 1998; Toomre et al., 1999), and disruption of the microtubule cytoskeleton and its motor proteins reduces the efficiency of apical and basolateral protein delivery to their respective membrane domains (Rindler et al., 1987; Lafont et al., 1994; Grindstaff et al., 1998; Kreitzer et al., 2000; Jaulin et al., 2007). How release and transport of vesicles from the Golgi complex to the plasma membrane are coordinated with microtubule organization is unknown.

In the budding yeast *Saccharomyces cerevisiae*, polarized membrane growth is spatiotemporally coordinated by septins (Barral et al., 2000; Gladfelter et al., 2001), a family of conserved filamentous GTPases that associate with cell membranes and the cytoskeleton (Spiliotis and Nelson, 2006). In mammalian cells, septins bind to microtubules (Surka et al., 2002; Nagata et al., 2003; Spiliotis et al., 2005), but the functional significance of this association in interphase cells and the role of septins in the morphogenesis of polarized epithelia are unknown. Here, we examine the distribution and function of the mammalian SEPT2 with respect to the microtubule cytoskeleton of Madin-Darby canine kidney (MDCK) cells. We show that SEPT2 associates with a distinct subset of microtubule tracks and is required for efficient Golgi-to-plasma membrane transport and the morphogenesis of columnar-shaped epithelial cells.

S. Hunt and Q. Hu contributed equally to this paper.

Correspondence to Elias T. Spiliotis: eliass@stanford.edu; or W. James Nelson: wjnelson@stanford.edu

Abbreviations used in this paper: C-MBD-MAP4, C-terminal microtubule binding domain of microtubule-associated protein 4; GalTase, galactosyltransferase; gpi, glycosyl phosphatidylinositol; LDL-R, low density lipoprotein receptor; MAP, microtubule-associated protein; p75, neurotrophin receptor protein 75; PKD, protein kinase D1; polyGlu, polyglutamylated; VSV-G, vesicular stomatitis virus G protein.

The online version of this paper contains supplemental material.

The Journal of Cell Biology, Vol. 180, No. 2, January 28, 2008 295–303
http://www.jcb.org/cgi/doi/10.1083/jcb.200710039

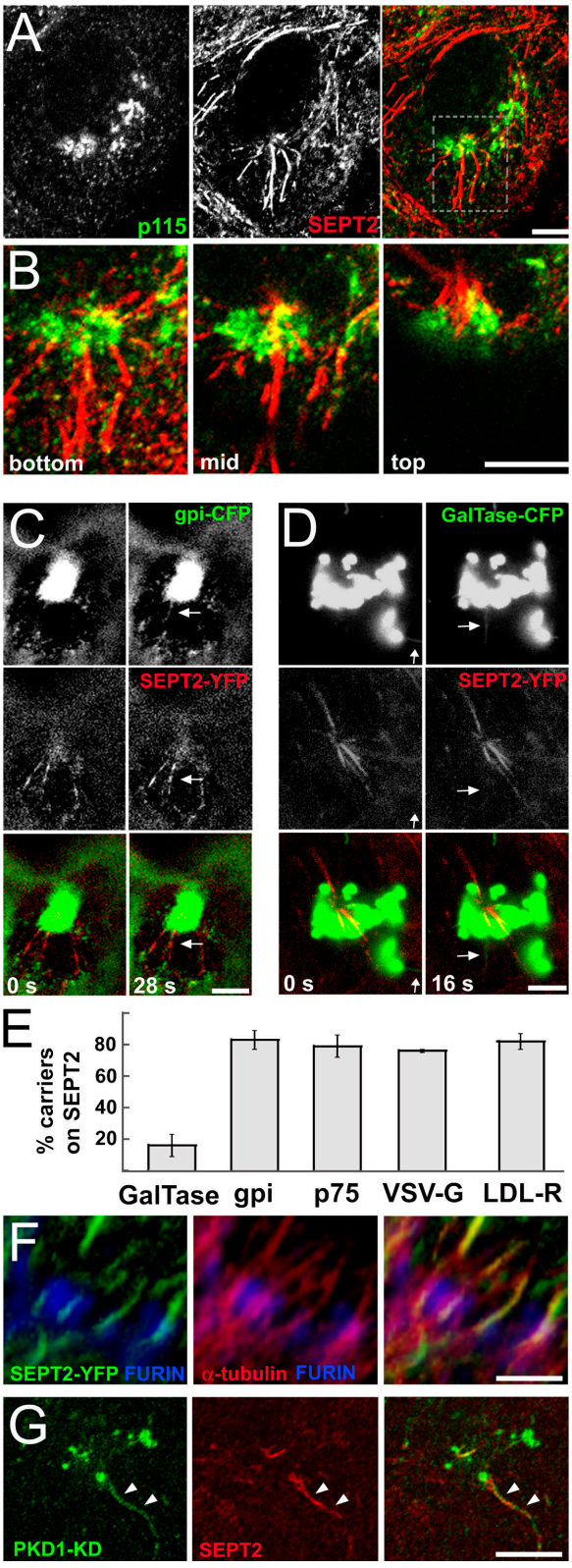

Figure 1. **SEPT2 fibers localize to TGN sites of apical and basolateral protein export.** (A and B) Subconfluent monolayers of MDCK cells were stained with SEPT2 and p115 antibodies, and imaged by confocal microscopy. Optical sections from the bottom, middle, and top of the highlighted Golgi region are shown at higher magnification (B). (C and D) MDCK-SEPT2-YFP cells were transiently transfected with gpi-CFP or GalTase-CFP, and imaged by time-lapse microscopy at 37°C. Non-neighbor deconvolution was applied and linear dynamic ranges were renormalized equally across the entire image to enhance the fluorescence intensity of tubular–vesicular structures. Arrows point to tubular vesicular elements extending from the Golgi complex. (E) Tubular–vesicular carriers containing CFP-tagged gpi, GalTase, VSV-G, and p75 were scored for overlap with SEPT2-YFP fibers (n = 80–100; mean values ± SEM from three independent experiments). (F) 3D-rendered confocal images of a Golgi region from MDCK-SEPT2-YFP cells stained with α-tubulin and furin convertase antibodies. (G) HeLa cells were transfected with the protein kinase D1 mutant PKD-K618N (PKD1-KD) tagged with GST. Cells were stained with GST and SEPT2 antibodies. Arrowheads point to a PKD-K618N–containing tubular extension. Bars, ~5 μm.

Results and discussion

Immunofluorescence microscopy of nonpolarized MDCK cells with antibodies to SEPT2 and the Golgi resident protein p115 revealed a juxtanuclear tuft of SEPT2 fibers closely apposed to the Golgi complex (Fig. 1, A and B). SEPT2 fibers co-aligned with microtubules (Fig. S1 A, available at http://www.jcb.org/cgi/content/full/jcb.200710039/DC1), and their distribution was dependent on microtubule structural integrity (Fig. S1 B). Because formation and transport of Golgi-derived vesicles occur along microtubules (Hirschberg et al., 1998; Toomre et al., 1999), we determined if SEPT2 localized to sites of vesicle export from the Golgi complex. We used high resolution live-cell imaging of MDCK cells that stably expressed a YFP-tagged SEPT2 at sub-endogenous levels (Spiliotis et al., 2005) and transiently co-expressed marker proteins of either the apical (CFP-tagged glycosyl phosphatidylinositol [gpi] or neurotrophin receptor protein 75 [p75]) or basolateral membrane (CFP-tagged vesicular stomatitis virus G protein [VSV-G] or low density lipoprotein receptor [LDL-R]). Note that SEPT2-YFP fibers colocalized with microtubules around the TGN similar to endogenous SEPT2 (Fig. 1 F). Strikingly, the majority of tubular–vesicular carriers containing apical (Fig. 1 C; Video 1 and Fig. S2, B and D) or basolateral marker proteins (Fig. S2, C and E) exited the Golgi complex along SEPT2-YFP fibers (Fig. 1 E). In contrast, membrane tubules containing a TGN resident protein (galactosyltransferase; GalTase) rarely overlapped with SEPT2-YFP fibers (Fig. 1, D and E; Video 2; Fig. S2 A).

In some instances SEPT2-YFP was not static but traversed the cytoplasm as tubular–vesicular elements (Video 3) with instantaneous velocities (0.38 ± 0.16 μm/s; n = 33) similar to those of kinesin-driven vesicles (Toomre et al., 1999). Consistent with this observation, and with septin binding to membrane phosphoinositides (Zhang et al., 1999) and synaptic vesicles (Beites et al., 1999), SEPT2 cofractionated with vesicle membranes that contained exocytic cargo (E-cadherin) and the small GTPase Rab8 (Fig. S3). SEPT2 also colocalized with Golgi-derived membrane tubules induced by expression of the inactive form of protein kinase D1 (PKD-K618N; Fig. 1 G), which blocks fission from the TGN of vesicles that are specifically destined for the plasma membrane (Liljedahl et al., 2001).

To test if SEPT2 is required for vesicle transport from the TGN to the plasma membrane, SEPT2 organization was disrupted by microinjecting cells with anti-SEPT2 IgGs and examining the effects on trafficking of the basolateral membrane marker VSV-G (ts045-VSV-G-YFP) and the apical membrane marker p75-GFP. In the presence of anti-SEPT2 IgGs, delivery

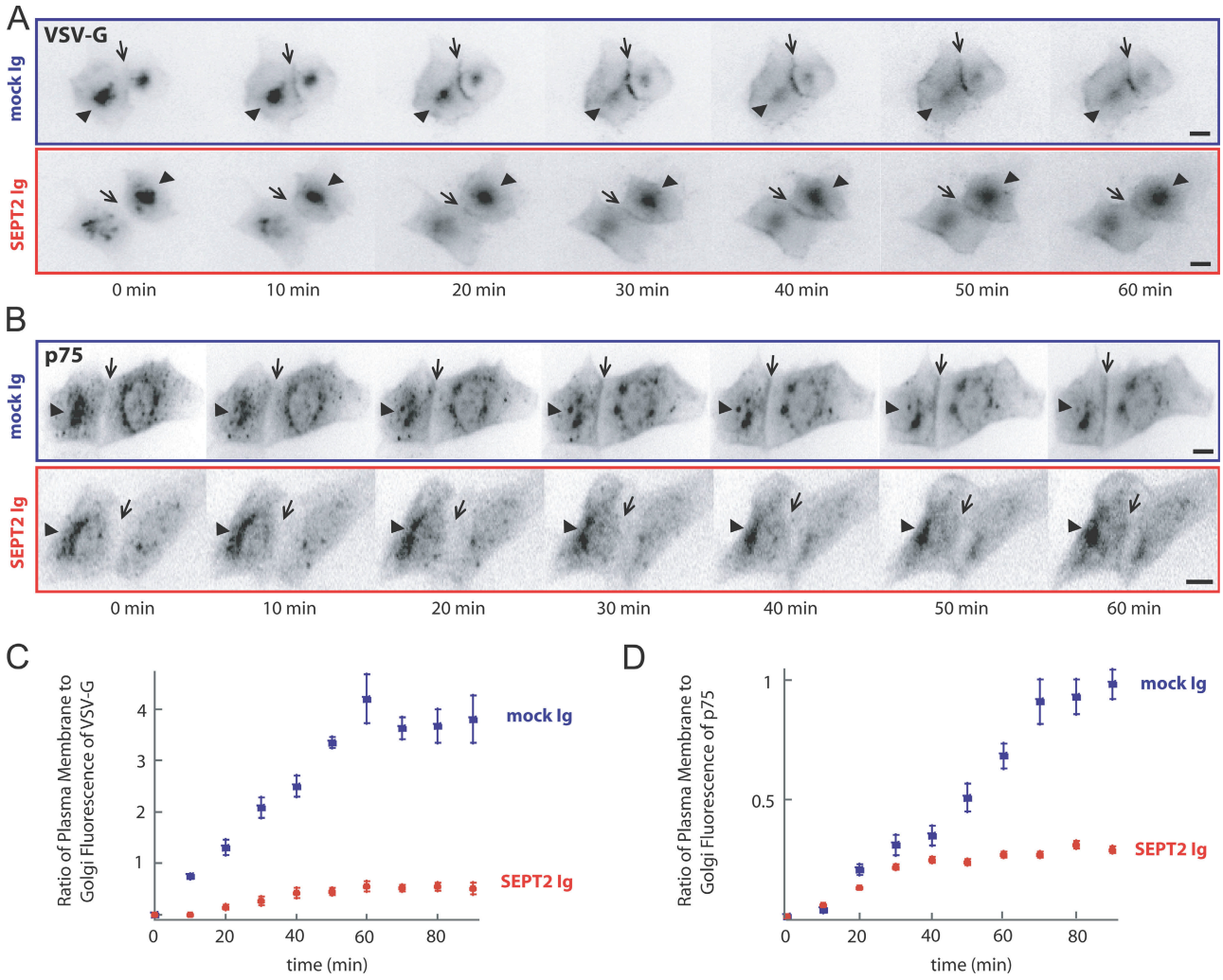

Figure 2. **SEPT2 is required for efficient Golgi-to-plasma membrane transport of basolateral and apical membrane proteins.** (A and B) Preimmune (mock; blue) or anti-SEPT2 (red) IgGs were microinjected into MDCK cells with plasmid vectors encoding for the temperature-sensitive mutant of the basolateral membrane protein VSV-G (ts045-VSV-G-YFP; A) or the apical protein p75-GFP (B). After accumulation of tsO45-VSV-G-YFP and p75-GFP in the Golgi complex at 19°C, live cells were imaged at 32°C. Arrows point to the plasma membrane of cell–cell contacts; arrowheads point to juxtanuclear Golgi regions. Bars, ~5 μm. (C and D) Net fluorescence intensities of cell surface (plasma membrane) and juxtanuclear Golgi regions were measured. Scatter plots show ratios (mean values ± SEM; *n* = 6) of plasma membrane to Golgi fluorescence for ts045-VSV-G-YFP– (C) and p75-GFP–expressing cells (D). Data are representative of three different experiments.

of ts045-VSV-G-YFP (Fig. 2, A and C) and p75-GFP (Fig. 2, B and D) from the Golgi to the plasma membrane was greatly reduced compared with that in the presence of control IgGs.

Co-alignment of SEPT2 with microtubules near the TGN (Fig. 1 F and Fig. S1 A) raised the possibility that SEPT2 might enhance vesicle transport on a qualitatively and/or functionally distinct subset of microtubule tracks. Immunofluorescence with antibodies to acetylated and detyrosinated tubulin revealed little or no colocalization between these post-translationally modified microtubules and SEPT2 fibers (unpublished data). In contrast, the preponderance of juxtanuclear/Golgi-proximal SEPT2 fibers colocalized with microtubules composed of polyglutamylated (polyGlu) tubulin (Fig. 3 A), which contains C-terminal side chains with 2–6 glutamate residues (Edde et al., 1990). When levels of SEPT2 were reduced by SEPT2 siRNAs, there was a concomitant decrease in the level of polyGlu microtubules (Fig. 3, B and E), indicating that SEPT2 is required for the maintenance of polyGlu microtubules. To further test whether SEPT2 is required for tubulin polyglutamylation, SEPT2 was buffered away from microtubules by overexpressing its cytoplasmic binding partner MAP4-GFP (Kremer et al., 2005). Excess cytoplasmic MAP4-GFP (high levels of expression; Fig. 3, C and F) not only eliminated SEPT2 association with microtubules as revealed by loss of juxtanuclear/Golgi-proximal SEPT2 fibers, but also decreased the level of polyGlu microtubules (Fig. 3, C and F). These effects were specific for MAP4 because overexpression of the neuronal MAP1B (Ding et al., 2002) (Fig. 3 D) or MAP8 (unpublished data) light chains did not disrupt SEPT2 fibers or polyGlu microtubules.

We next examined whether loss of SEPT2 fibers and polyGlu microtubules affected vesicular transport between the Golgi and the plasma membrane. Indeed, loss of SEPT2 fibers and polyGlu microtubule tracks upon MAP4-GFP overexpression resulted in decreased delivery of ts045-VSV-G-YFP to the

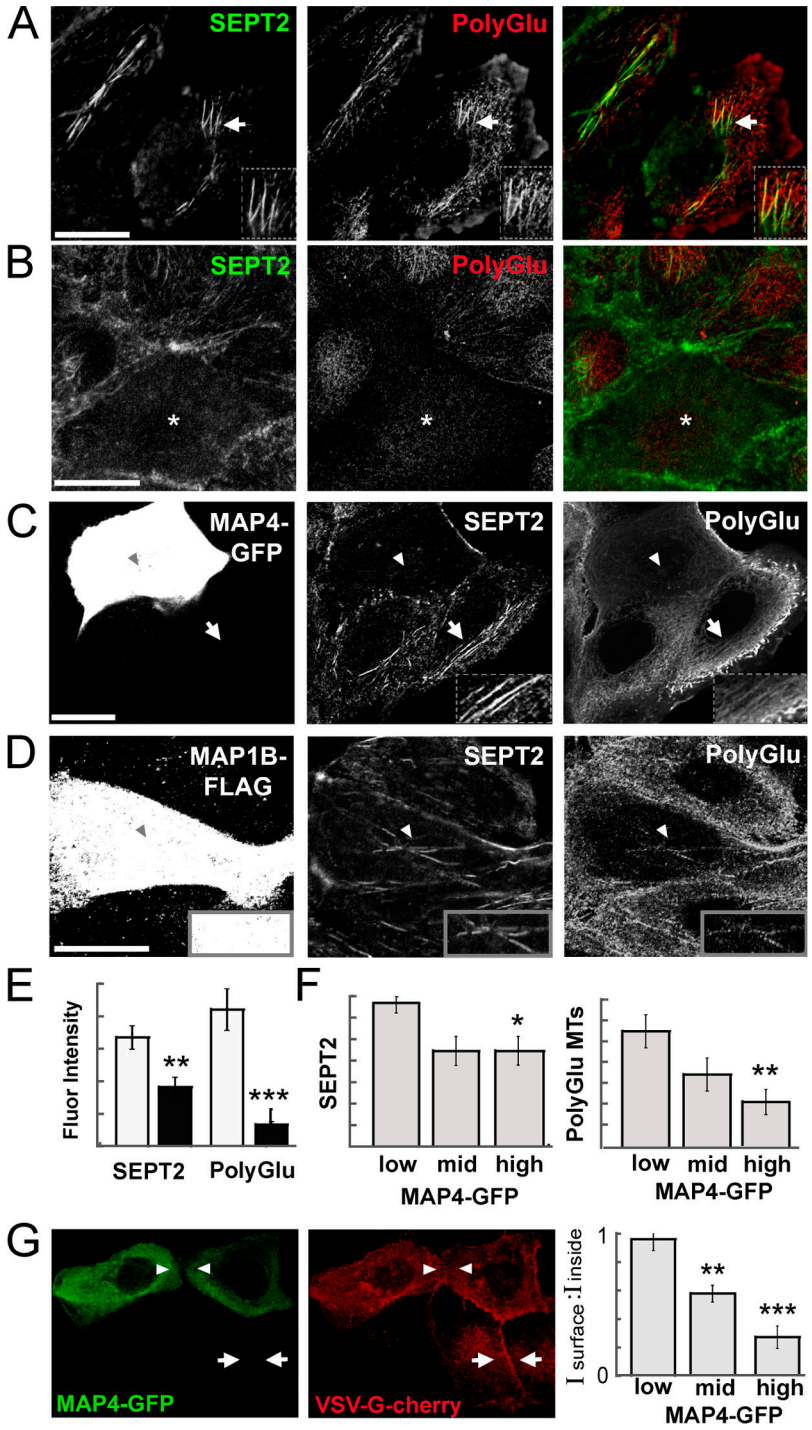

Figure 3. **SEPT2 fibers colocalize with, and are required for, polyglutamylated microtubule tracks.** (A and B) Untreated (A) and SEPT2-siRNA-treated (B) MDCK cells were stained with SEPT2 and polyGlu (≥2 glutamate residues) tubulin (mAb B3) antibodies and imaged by confocal microscopy. In A, arrows point to juxtanuclear/Golgi SEPT2 filaments that colocalize with polyGlu-microtubule tracks (see insets for higher magnification). In B, the asterisk marks a SEPT2-depleted cell. (C and D) MDCK cells were transfected with MAP4-GFP and FLAG-tagged MAP1B light chain (MAP1B-FLAG), and stained with SEPT2, polyGlu-tubulin, and FLAG antibodies. Arrows point to polyGlu microtubules and SEPT2 filaments (see insets for higher magnification), and arrowheads point to the juxtanuclear/Golgi regions of MAP-expressing cells. (E) Bar graph shows mean SEPT2 and polyGlu tubulin fluorescence (± SEM) in control (white columns; $n = 11$) and SEPT2 (black columns; $n = 13$) siRNA-treated cells. **, $P = 0.0042$; ***, $P < 0.0001$. (F) Bar graphs show mean SEPT2 ($n = 19$) and polyGlu tubulin ($n = 25$) fluorescence (± SEM) as a function of MAP4-GFP expression after binning GFP fluorescence into low, mid, and high range values. *, $P = 0.04$; **, $P = 0.003$. (G) MDCK cells were transfected with MAP4-GFP and ts045-VSV-G-cherry at 41°C and then shifted to 32°C for 1.5 h. Arrowheads (MAP4-GFP-expressing cells) and arrows (nonexpressing cells) point to the plasma membrane at cell–cell contacts. Bar graph shows mean (± SEM) ratios of plasma membrane to intracellular fluorescence for cells ($n = 30$) with low, middle, and high levels of MAP4-GFP expression from three independent experiments. **; $P = 0.001$; ***; $P < 0.0001$.

plasma membrane (Fig. 3 G). Direct disruption of SEPT2 fibers in cells cotransfected with SEPT2 siRNAs and ts045-VSV-G-YFP also reduced Golgi-to-plasma membrane transport of VSV-G (ratio of plasma membrane [PM] to intracellular [IC] fluorescence of 0.6 ± 0.04 [$n = 21$] vs. 1 ± 0.1 [$n = 9$] in control cells; $P < 0.0001$). However, cotransfection of a mixture of SEPT2 and MAP4 siRNAs resulted in an intermediate VSV-G delivery phenotype (PM:IC fluorescence 0.81 ± 0.1 [$n = 22$]; $P < 0.003$), indicating that SEPT2 and MAP4 counteract each other in regulating vesicle transport along microtubules. Therefore, in addition to the previously characterized role of cytoplasmic septins in sequestering MAP4 from microtubules (Kremer et al., 2005), which controls the stability of microtubules, microtubule-associated SEPT2 is required for the maintenance of a distinct subset of microtubules (polyGlu microtubules) that facilitate efficient vesicle transport.

To further examine whether the polyGlu side chains of tubulin or polyGlu tubulin-bound SEPT2 directly affect MAP4–tubulin binding, we used a competitive blot overlay assay, which has been used previously to map tubulin binding sites of motors and MAPs and quantitatively examine the effect of tubulin polyglutamylation on their binding (Larcher et al., 1996;

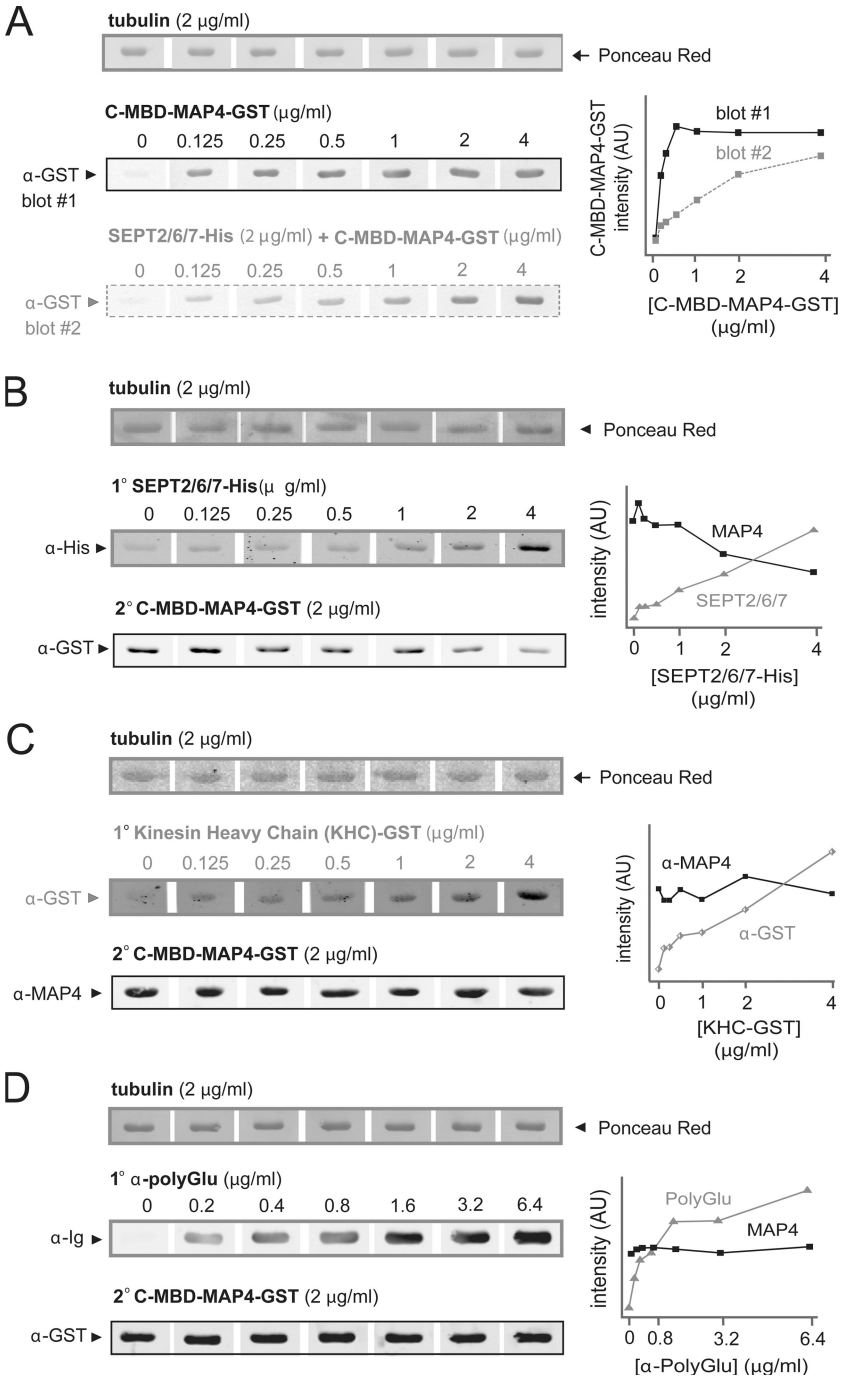

Figure 4. **Tubulin-bound SEPT2 complexes inhibit binding of the microtubule-binding domain of MAP4 (C-MBD-MAP4) to tubulin.** Equal amounts (2 μg) of purified tubulin were separated by 10% SDS-PAGE, transferred to nitrocellulose, and stained with Ponceau red. (A) Tubulin-containing strips were overlaid with increasing concentrations (0–4 μg/ml) of GST-tagged C-MBD-MAP4 directly (solid line; blot #1), or first overlaid with His-tagged SEPT2/6/7 (2 μg/ml) and then increasing concentrations of C-MBD-MAP4-GST (dotted line; blot #2). (B) Tubulin-containing strips were overlaid with increasing concentrations (0–4 μg/ml) of His-SEPT2/6/7 (1° overlay) and then with C-MBD-MAP4-GST (2 μg/ml; 2° overlay). (C) Tubulin strips were overlaid with increasing concentrations (0–4 μg/ml) of GST-tagged kinesin heavy chain (KHC-GST; 1° overlay) and then, with C-MBD-MAP4-GST (2 μg/ml; 2° overlay). (D) Tubulin was overlaid with an increasing concentration (0–6.4 μg/ml) of anti-polyGlu tubulin (mAb B3; 1° overlay) and then with C-MBD-MAP4-GST (2 μg/ml; 2° overlay). Tubulin-bound proteins were detected with GST, His, MAP4, and Ig antibodies. Band intensities were quantified and plotted against protein concentrations.

Bonnet et al., 2001). Overlaying purified brain tubulin (high polyGlu content) with recombinant SEPT2/6/7 complex decreased tubulin binding of the C-terminal microtubule binding domain of MAP4 (C-MBD-MAP4) (Fig. 4 A); note that in vivo SEPT2 functions as a heterotrimer with SEPT6 and SEPT7 (SEPT2/6/7 complex; see Kinoshita et al., 2002). SEPT2 complexes also decreased C-MBD-MAP4 binding to tubulin in a concentration-dependent manner (Fig. 4 B). In contrast, increasing concentrations of anti-polyGlu antibody (Fig. 4 D) or kinesin heavy chain (Fig. 4 C) did not interfere with binding of C-MBD-MAP4 to tubulin. Thus, polyGlu tubulin-bound SEPT2 can directly interfere with MAP4–tubulin binding.

Having shown that SEPT2 plays roles in vesicular transport, we tested whether SEPT2 is required for the establishment of epithelial membrane polarity and columnar cell shape. We depleted endogenous SEPT2 from nonpolarized, "contact-naïve" MDCK cells with siRNAs, and then assayed cell polarity and shape in monolayers of polarized cells grown on filters (Fig. 5, A and B). In contrast to the columnar morphology of cells treated with control siRNAs, SEPT2-depleted cells lacked an apical dome and honeycomb morphology characteristic of a polarized, columnar epithelium (Fig. 5 C). Significantly, SEPT2-depleted cells were elongated along their long axis and were shorter compared with control cells (Fig. 5 D). These defects

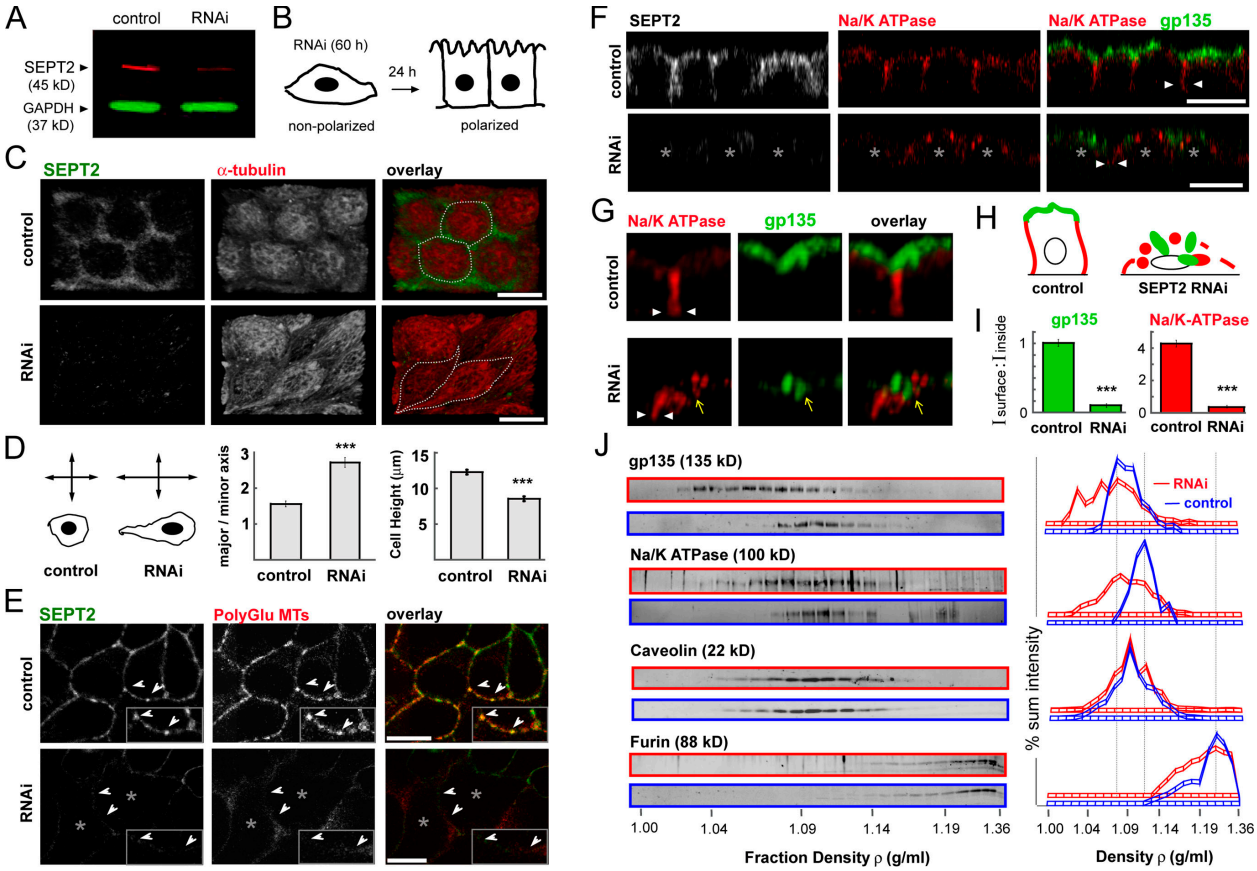

Figure 5. **SEPT2 is required for the morphogenesis of polarized, columnar-shaped epithelia.** (A) Non-polarized, "contact-naïve" MDCK cells were transfected with control and SEPT2 siRNAs for 60 h. Cell extracts were analyzed by SDS-PAGE and Western blotting with antibodies to SEPT2 (red) and glyceraldehyde-3-phosphate dehydrogenase (GAPDH; green). (B) Schematic of the experimental setup. (C) Representative dorsal views of 3D-rendered confocal images of MDCK cells stained for SEPT2 and α-tubulin. (D) Representative contour sketches of control and SEPT2-depleted cells. The ratios (mean ± SEM) of lengths of major-to-minor cell axes are shown for control (n = 33) and SEPT2-depleted (n = 30) cells from three independent experiments ($P < 0.0001$). Cell heights were measured from cross sections (xz) of confocal images and their values (mean ± SEM) are shown for control (n = 20) and SEPT2-depleted (n = 20) cells ($P < 0.0001$). (E) Representative mid-section confocal images of MDCK cells stained for SEPT2 and polyGlu tubulin; fixation/permeabilization conditions differed from those in F (see Materials and methods). Arrowheads point to SEPT2 and polyGlu microtubules that run parallel to the lateral membrane in the apicobasal axis. (F) Representative confocal cross sections (xz) of MDCK cells stained for SEPT2, Na/K-ATPase, and gp135/podocalyxin. Asterisks outline SEPT2-depleted cells; arrowheads point to lateral cell–cell contacts. (G) High resolution 3D-rendered images of the regions outlined by arrows in F. Yellow arrows point to punctate structures containing gp135/podocalyxin and Na/K-ATPase. (H) Cartoons of Na/K-ATPase (green) and gp135/podocalyxin (red) localizations in control and SEPT2-depleted cells. (I) Apical (gp135/podocalyxin) and basolateral (Na/K-ATPase) membrane and intracellular fluorescence intensities were measured from confocal cross sections (xz) of control (n = 23) and SEPT2-depleted (n = 23) cells. Bar graphs show ratios (mean values ± SEM) of plasma membrane to intracellular fluorescence from three independent experiments (***, $P < 0.0001$). (J) Post-nuclear homogenates from control (red) and SEPT2-depleted (blue) MDCK monolayers separated in iodixanol (OptiPrep) gradients, and analyzed by SDS-PAGE and blotted with antibodies to gp135/podocalyxin (apical), Na/K-ATPase (basolateral), caveolin (apical and basolateral), and furin convertase (TGN). Protein band intensities were plotted as a percentage of their sum intensity. Vertical lines demarcate the peak fractions of apical, basolateral, and Golgi proteins in gradients from control cells. Data are representative of three independent experiments.

correlated with a lack of vertically oriented polyGlu microtubules; note that in columnar-shaped control cells polyGlu microtubules colocalized with SEPT2 fibers parallel to the lateral membrane in the apicobasal cell axis (Fig. 5 E). Moreover, in SEPT2-depleted cells, levels of endogenous apical (gp135/podocalyxin) and basolateral (Na/K-ATPase) membrane markers were significantly reduced from their respective membrane domains (Fig. 5, F and I), and these proteins accumulated intracellularly in punctate structures (Fig. 5, G and H); this was not due to loss of the diffusion barrier between the apical and basolateral membrane domains as tight junctions were unaffected in SEPT2-depleted cells (unpublished data). In OptiPrep density gradients of membranes from control and SEPT2 siRNA-treated cells (Fig. 5 J), the distribution of membranes containing gp135/podocalyxin and Na/K-ATPase shifted toward fractions of low buoyant density (ρ = 1.03–1.08 g/ml) compared with controls. These fractions did not contain the TGN resident protein furin (Fig. 5 J) and their low densities resembled those of post-Golgi vesicle membranes (Wandinger-Ness et al., 1990; Deretic and Papermaster, 1991), which is consistent with the accumulation of gp135/podocalyxin and Na/K-ATPase in punctate intracellular structures (Fig. 5 G). Note that caveolin, which traffics from the Golgi to both the apical and basolateral membranes in stable microdomains distinct from the dynamic mechanisms of vesicle formation that characterize most membrane proteins (Tagawa et al., 2005), was unaffected by SEPT2 depletion (Fig. 5 J).

Based on these data, we suggest that SEPT2 is required for efficient Golgi-to-plasma membrane transport of vesicles

containing apical or basolateral membrane proteins. This is supported by: (1) presence of SEPT2 at TGN sites of plasma membrane protein export (Fig. 1); (2) decreased post-Golgi vesicle traffic in nonpolarized MDCK cells upon microinjection of function-blocking SEPT2 antibodies (Fig. 2); and (3) reduced membrane growth (Fig. 5, G and H) and columnarization (Fig. 5, C and D) of MDCK cell monolayers upon SEPT2 depletion. Although SEPT2 is involved in microtubule-dependent vesicle transport at TGN exit sites, we cannot exclude the possibility that SEPT2 also functions in vesicular transport from and to post-Golgi compartments (e.g., recycling endosomes) en route to the plasma membrane. Recent studies indicate that apical and basolateral proteins traffic through transport intermediates upon exit from the TGN (Ang et al., 2004; Fields et al., 2007; Gravotta et al., 2007). Interestingly, SEPT2 localization to endosomes and cell–cell junctions has been observed in MDCK cells by immuno-EM (unpublished data). Future studies will test whether septins regulate vesicle transport at these sites of membrane fission and fusion.

Similar to the Ras-like (e.g., Rab, Rho/Rac) and myosin-kinesin superfamilies of P-loop NTPases, septins comprise a unique superfamily of GTPases (Leipe et al., 2002). Although cytoplasmic septin complexes have been shown to regulate microtubule stability (Kremer et al., 2005), the function of the microtubule-associated, filamentous septins is unknown. We suggest that SEPT2 regulates the efficiency of vesicle transport by antagonizing MAP4, whose inhibitory role in vesicle transport is independent of its role in microtubule stability (Bulinski et al., 1997). Because microtubule-associated proteins inhibit the binding of TGN-derived vesicles to microtubules in vitro (Van der Sluijs et al., 1990) and membrane motility and traffic in vivo (Bulinski et al., 1997), we suggest that SEPT2 binding to polyglutamylated microtubules specifies a functionally distinct subset of microtubule tracks on which "fast track" vesicle transport occurs without the impediment of MAP "speed bumps." Therefore, the balance between the levels of polyGlu microtubules, SEPT2, and MAP4 may control the amount of vesicle transport to the plasma membrane. For example, different amounts of vesicle transport may be required for rapid membrane growth during morphogenesis of a columnar epithelium compared with those required to maintain homeostasis or in response to physiological stress (wound healing). This type of regulation may be important in other cell types, as microtubule-dependent vesicle transport in neurons requires polyGlu microtubules (Ikegami et al., 2007) and the dissociation of MAPs from microtubules (Mandelkow et al., 2004).

Materials and methods

Cell culture and DNA constructs

HeLa and MDCK clone II cells were maintained as described previously (Spiliotis et al., 2005). The plasmid vector encoding for ts045-VSVG3-SP-cherry was constructed by subcloning mCherry into pVSVG3-SP-YFP-N1 (a gift from K. Simons, Max Planck Institute of Molecular Cell Biology and Genetics, Dresden, Germany).

Plasmid DNA and siRNA transfections

Plasmids for ts045-VSVG3-SP-cherry, GST-tagged PKD1-K618N (a gift from V. Malhotra, CRG, Barcelona, Spain), MAP4-GFP (a gift from I. Macara, University of Virginia, Charlottesville, VA), and FLAG-tagged MAP1B and MAP8 (gifts from Y. Yang, Stanford University, Stanford, CA) were transfected using the Lipofectamine 2000 reagent (Invitrogen). MDCK cells were transfected with siCONTROL nontargeting siRNA #1 (Dharmacon RNA Technologies), MAP4 (ON-TARGET plus SMART pool; Dharmacon RNA Technologies), and SEPT2 siRNA oligonucleotides as described previously (Spiliotis et al., 2005).

Immunofluorescence microscopy

Subconfluent cell monolayers (Figs. 1, 3, and S1) were fixed with warm PHEM (60 mM Pipes-KOH, pH 6.9, 25 mM Hepes, 10 mM EGTA, and 1 mM $MgCl_2$) containing 3% paraformaldehyde (PFA; EM Sciences) and 0.1% Triton X-100, and stained with antisera to SEPT2 (N5N; rabbit polyclonal), α-tubulin (DM1A; Sigma-Aldrich), p115 (a gift from S. Pfeffer, Stanford University), furin convertase (ABR), GST (mAb B-14; Santa Cruz Biotechnology, Inc.), polyglutamylated tubulin (IgM clone B3; Sigma-Aldrich), FLAG (mAb M2; Sigma-Aldrich), and with secondary FITC- or Rhodamine red X–conjugated $F(ab')_2$ goat or donkey anti–mouse and anti–rabbit IgGs, Rhodamine red X–conjugated $F(ab')_2$ goat anti–mouse IgM and Cy5-conjugated $F(ab')_2$ donkey anti–rabbit IgG (Jackson ImmunoResearch Laboratories).

Confluent MDCK monolayers grown on Transwell filters (Figs. 5 F and S4) were fixed in PBS containing 3% PFA and stained with antibodies to SEPT2, gp135/podocalyxin (3F2/D8 mouse hybridoma supernatant), and Na/K-ATPase (chicken polyclonal; Novus). To stain for α-tubulin and polyGlu tubulin (Fig. 5, C and E), cells were fixed with warm microtubule stabilizing buffer (80 mM Pipes-KOH; pH 6.8, 5 mM EDTA, and 2 mM $MgCl_2$) containing 0.5% Triton X-100 and 0.3% glutaraldehyde (EM Sciences).

Samples were imaged in Vectashield mounting medium (Vector Laboratories) with a confocal laser scanning microscope (LSM 510; Carl Zeiss, Inc.) by obtaining 0.4–0.8-μm optical sections with a 100× 1.4 NA oil objective. Fluorescence quantifications (Fig. 3) were performed after importing LSM images into Slidebook 4.2 software (Intelligent Imaging Innovations). Data were binned into three categories based on the range of GFP fluorescence intensities; 0–20 arbitrary units (low; e.g., top right cell in Fig. 3 G), 20–40 arbitrary units (mid; e.g., top left cell in Fig. 3 G), or >40 arbitrary units (high; e.g., top cell in Fig. 3 C). Cell heights were measured using LSM software (Carl Zeiss, Inc.). The lengths of the major and minor cell axes were automatically calculated using the ellipse best-fit module of the Slidebook 4.2 software. 3D volume rendering and fluorescence quantifications (Fig. 5 and S4) were performed with Volocity 4.2 software (Improvision). Data were statistically analyzed using an automated unpaired *t* test (http://www.physics.csbsju.edu/stats/t-test.html). Image manipulations were limited to renormalization of linear dynamic ranges and applied equally across the entire image. No gamma corrections were applied.

Microinjections and live-cell imaging

Preimmune and anti-SEPT2 (N5N; 0.5–1 mg/ml needle concentration) sera were dialyzed, concentrated on Microcon 50.000 MW columns (Millipore), mixed with plasmid DNA in 10 mM Hepes, 140 mM KCl, pH 7.4, and injected into the cytoplasm and nuclei of cells with an Eppendorf microinjection system. In Fig. 1, MDCK-SEPT2-YFP cells were transfected with plasmids for CFP-tagged p75, LDL-R (gifts from E. Rodriguez-Boulan, Weill Medical College of Cornell University, New York, NY), gpi (a gift from M. Edidin, The Johns Hopkins University, Baltimore, MD), VSV-G or GalTase (gifts from J. Lippincott-Schwartz, NICHD, National Institutes of Health, Bethesda, MD). In Fig. 2, tsO45-VSV-G-YFP–injected cells were maintained at 41°C for 2 h before shifting the temperature to 32°C for 10 min, and then to 19°C for 30 min in the presence of cycloheximide (50 μg/ml); p75-GFP-injected cells were maintained at 19°C before transferring to media with cycloheximide for 30 min. Subsequently, cells were imaged in cycloheximide (10 μg/ml) containing media.

Cells were imaged in phenol red–free DME supplemented with 25 mM Hepes using the Marianas system (Intelligent Imaging Innovations) equipped with a 175-Watt Xenon light source, a dual galvanometric filter changer with CFP and YFP excitation/emission filters, CoolSNAP HQ interline CCD camera, and a Plan-Apo 100× 1.4 NA oil objective. No-neighbors deconvolution and post-acquisition analysis were performed using Slidebook 4.2. Sum fluorescence intensities for Golgi and plasma membrane regions were measured after image segmentation using the mask and pencil tools of Slidebook. Spatial overlap between tubular–vesicular structures and SEPT2 filaments was determined by the overlap of YFP and CFP fluorescence.

Recombinant proteins and blot overlay assays

Bovine brain tubulin and GST-human kinesin heavy chain motor domain were purchased from Cytoskeleton, Inc. The C-terminal microtubule-binding domain of human MAP4 (aa 654–1090; a gift from I. Macara) and

His-SEPT2/6/7 complexes were purified as previously described (Kinoshita et al., 2002; Kremer et al., 2005).

In blot overlay assays, brain tubulin was separated by 10% SDS-PAGE and transferred onto nitrocellulose membranes, which were stained with Ponceau S (Sigma-Aldrich). Membranes were scanned, cut into strips, destained, and incubated overnight at 4°C in blocking buffer (10 mM Tris HCl, pH 6.8, 150 mM NaCl, 1 mM DTT, 0.1% Tween 20, 5% nonfat dry milk, and 0.5% BSA). Recombinant proteins and antibodies were diluted in blocking buffer and overlaid onto membrane strips. To visualize tubulin-bound proteins, membranes were washed with TBS, 0.1% Tween 20, and incubated in the same buffer containing 2% BSA and antibodies. Blots were subsequently incubated with secondary AlexaFluor 680 and IRDye800-conjugated antibodies and scanned in a Li-COR infrared imager. Quantification of protein bands was performed with the Odyssey Infrared Imaging System (LI-COR Biosciences).

MDCK cell fractionation on OptiPrep density gradients and Western blotting

Non-polarized "contact naïve" MDCKs were transfected with siCONTROL and SEPT2 siRNAs, and passaged twice while being maintained in regular medium for 60 h. Cells (15×10^6) were plated onto collagen-coated 75-mm Transwell filters (Costar) for 24 h, and ball-bearing homogenized in buffer I (25 mM sucrose, 20 mM Hepes KOH, pH 7.1, 90 mM potassium acetate, 2 mM magnesium acetate, 2 mM Pefabloc, and protease inhibitors). Post-nuclear supernatants were adjusted with buffer I and OptiPrep (Axis-Shield) to 30% (wt/vol) iodixanol, overlaid with equal volumes of 20 and 10% iodixanol solutions, and centrifuged at 350,000 *g* for 3 h in a VTI 65.1 rotor (Beckman Coulter). Equal volume fractions were collected from the top ($\rho \sim 1$ g/ml) through the bottom ($\rho \sim 1.3$ g/ml) of the gradient, and the refractive index (η) of each fraction was measured using a refractometer (Bausch & Lomb). Densities were determined in g/ml [$\rho = (\eta \times 3.443) - 3.599$]. For the linear portions of these gradients (fractions 1–23), the densities for the same numbered fractions were equivalent across gradients. Fractions were boiled in SDS sample buffer and analyzed by SDS-PAGE and immunoblotting with antibodies to gp135/podocalyxin, Na/K-ATPase (α3NKA), caveolin (Transduction Laboratories), furin convertase (ABR-Affinity BioReagents), glyceraldehyde-3-phosphate dehydrogenase (6C5; Abcam), and AlexaFluor 680 goat anti–rabbit and anti–mouse IgGs (Invitrogen). Scanning of membranes and quantification of protein bands were performed with the Odyssey Infrared Imaging System (LI-COR Biosciences).

Subcellular fractionation of vesicle membranes

MDCK cells were homogenized in buffer containing 10 mM Hepes-NaOH, pH 7.4, 140 mM KCl, 5 mM EGTA, 1 mM DTT, 2 mM Pefabloc, and protease inhibitors. Post-18,000 *g* supernatants were adjusted with OptiPrep to 30% iodixanol, overlaid with equal volumes of 25 and 5% iodixanol, and centrifuged at 300,000 *g* for 3 h to obtain a fourth layer (clathrin-free vesicle fraction) at the interphase between the 5 and 25% iodixanol solutions. Vesicle fractions were drawn with a syringe and centrifuged at 100,000 *g* for 1 h in a TL-100 Tabletop Ultracentrifuge (Beckman Coulter). Membrane pellets and cytosolic supernatants were boiled in SDS sample buffer before SDS-PAGE and immunoblotting with antibodies to E-cadherin (rabbit polyclonal E2), clathrin heavy chain (Clone 23; BD Biosciences), Rab8 (BD Biosciences), and membrin (Assay Designs).

Online supplemental material

Fig. S1 shows localization of SEPT2 fibers with respect to microtubules in untreated and nocodazole-treated MDCK cells. Fig. S2 is a gallery of still images from time-lapse movies of SEPT2-YFP and Golgi-derived vesicular–tubular carriers containing CFP-tagged GalTase, gpi, ts045-VSV-G, p75, and LDL-R. Fig. S3 demonstrates SEPT2 co-fractionation with vesicle membranes. Videos 1 and 2 are time-lapse movies of SEPT2-YFP and Golgi-derived vesicular carriers that contain CFP-tagged gpi and GalTase, respectively. Video 3 shows vesicular movement of SEPT2-YFP. Online supplemental material is available at http://www.jcb.org/cgi/content/full/jcb.200710039/DC1.

We thank V. Varenika and members of the Nelson laboratory for technical help and advice; and Drs. S. Pfeffer, E. Rodriguez-Boulan, J. Lippincott-Schwartz, K. Simons, I. Macara, V. Malhotra, and Y. Yang for reagents.

This work was supported by NIH grant GM35527 (W.J. Nelson), a postdoctoral fellowship from the Jane Coffin Childs Fund for Medical Research (E.T. Spiliotis), and NIH MSTP (S.J. Hunt) and Cell and Molecular Biology (Q. Hu) training grants. Data cited as unpublished are available upon reader's request.

Submitted: 5 October 2007
Accepted: 28 December 2007

References

Ang, A.L., T. Taguchi, S. Francis, H. Folsch, L.J. Murrells, M. Pypaert, G. Warren, and I. Mellman. 2004. Recycling endosomes can serve as intermediates during transport from the Golgi to the plasma membrane of MDCK cells. *J. Cell Biol.* 167:531–543.

Barral, Y., V. Mermall, M.S. Mooseker, and M. Snyder. 2000. Compartmentalization of the cell cortex by septins is required for maintenance of cell polarity in yeast. *Mol. Cell.* 5:841–851.

Beites, C.L., H. Xie, R. Bowser, and W.S. Trimble. 1999. The septin CDCrel-1 binds syntaxin and inhibits exocytosis. *Nat. Neurosci.* 2:434–439.

Bonnet, C., D. Boucher, S. Lazereg, B. Pedrotti, K. Islam, P. Denoulet, and J.C. Larcher. 2001. Differential binding regulation of microtubule-associated proteins MAP1A, MAP1B, and MAP2 by tubulin polyglutamylation. *J. Biol. Chem.* 276:12839–12848.

Bulinski, J.C., T.E. McGraw, D. Gruber, H.L. Nguyen, and M.P. Sheetz. 1997. Overexpression of MAP4 inhibits organelle motility and trafficking in vivo. *J. Cell Sci.* 110:3055–3064.

Deretic, D., and D.S. Papermaster. 1991. Polarized sorting of rhodopsin on post-Golgi membranes in frog retinal photoreceptor cells. *J. Cell Biol.* 113:1281–1293.

Ding, J., J.J. Liu, A.S. Kowal, T. Nardine, P. Bhattacharya, A. Lee, and Y. Yang. 2002. Microtubule-associated protein 1B: a neuronal binding partner for gigaxonin. *J. Cell Biol.* 158:427–433.

Edde, B., J. Rossier, J.P. Le Caer, E. Desbruyeres, F. Gros, and P. Denoulet. 1990. Posttranslational glutamylation of alpha-tubulin. *Science.* 247:83–85.

Fields, I.C., E. Shteyn, M. Pypaert, V. Proux-Gillardeaux, R.S. Kang, T. Galli, and H. Folsch. 2007. v-SNARE cellubrevin is required for basolateral sorting of AP-1B-dependent cargo in polarized epithelial cells. *J. Cell Biol.* 177:477–488.

Gladfelter, A.S., J.R. Pringle, and D.J. Lew. 2001. The septin cortex at the yeast mother-bud neck. *Curr. Opin. Microbiol.* 4:681–689.

Gravotta, D., A. Deora, E. Perret, C. Oyanadel, A. Soza, R. Schreiner, A. Gonzalez, and E. Rodriguez-Boulan. 2007. AP1B sorts basolateral proteins in recycling and biosynthetic routes of MDCK cells. *Proc. Natl. Acad. Sci. USA.* 104:1564–1569.

Griffiths, G., and K. Simons. 1986. The trans Golgi network: sorting at the exit site of the Golgi complex. *Science.* 234:438–443.

Grindstaff, K.K., R.L. Bacallao, and W.J. Nelson. 1998. Apiconuclear organization of microtubules does not specify protein delivery from the trans-Golgi network to different membrane domains in polarized epithelial cells. *Mol. Biol. Cell.* 9:685–699.

Hirschberg, K., C.M. Miller, J. Ellenberg, J.F. Presley, E.D. Siggia, R.D. Phair, and J. Lippincott-Schwartz. 1998. Kinetic analysis of secretory protein traffic and characterization of golgi to plasma membrane transport intermediates in living cells. *J. Cell Biol.* 143:1485–1503.

Ikegami, K., R.L. Heier, M. Taruishi, H. Takagi, M. Mukai, S. Shimma, S. Taira, K. Hatanaka, N. Morone, I. Yao, et al. 2007. Loss of alpha-tubulin polyglutamylation in ROSA22 mice is associated with abnormal targeting of KIF1A and modulated synaptic function. *Proc. Natl. Acad. Sci. USA.* 104:3213–3218.

Jaulin, F., X. Xue, E. Rodriguez-Boulan, and G. Kreitzer. 2007. Polarization-dependent selective transport to the apical membrane by KIF5B in MDCK cells. *Dev. Cell.* 13:511–522.

Kinoshita, M., C.M. Field, M.L. Coughlin, A.F. Straight, and T.J. Mitchison. 2002. Self- and actin-templated assembly of Mammalian septins. *Dev. Cell.* 3:791–802.

Kreitzer, G., A. Marmorstein, P. Okamoto, R. Vallee, and E. Rodriguez-Boulan. 2000. Kinesin and dynamin are required for post-Golgi transport of a plasma-membrane protein. *Nat. Cell Biol.* 2:125–127.

Kremer, B.E., T. Haystead, and I.G. Macara. 2005. Mammalian septins regulate microtubule stability through interaction with the microtubule-binding protein MAP4. *Mol. Biol. Cell.* 16:4648–4659.

Lafont, F., J.K. Burkhardt, and K. Simons. 1994. Involvement of microtubule motors in basolateral and apical transport in kidney cells. *Nature.* 372:801–803.

Larcher, J.C., D. Boucher, S. Lazereg, F. Gros, and P. Denoulet. 1996. Interaction of kinesin motor domains with alpha- and beta-tubulin subunits at a tau-independent binding site. Regulation by polyglutamylation. *J. Biol. Chem.* 271:22117–22124.

Leipe, D.D., Y.I. Wolf, E.V. Koonin, and L. Aravind. 2002. Classification and evolution of P-loop GTPases and related ATPases. *J. Mol. Biol.* 317:41–72.

Liljedahl, M., Y. Maeda, A. Colanzi, I. Ayala, J. Van Lint, and V. Malhotra. 2001. Protein kinase D regulates the fission of cell surface destined transport carriers from the trans-Golgi network. *Cell.* 104:409–420.

Mandelkow, E.M., E. Thies, B. Trinczek, J. Biernat, and E. Mandelkow. 2004. MARK/PAR1 kinase is a regulator of microtubule-dependent transport in axons. *J. Cell Biol.* 167:99–110.

Matter, K., and I. Mellman. 1994. Mechanisms of cell polarity: sorting and transport in epithelial cells. *Curr. Opin. Cell Biol.* 6:545–554.

Mostov, K.E., M. Verges, and Y. Altschuler. 2000. Membrane traffic in polarized epithelial cells. *Curr. Opin. Cell Biol.* 12:483–490.

Musch, A. 2004. Microtubule organization and function in epithelial cells. *Traffic.* 5:1–9.

Nagata, K., A. Kawajiri, S. Matsui, M. Takagishi, T. Shiromizu, N. Saitoh, I. Izawa, T. Kiyono, T.J. Itoh, H. Hotani, and M. Inagaki. 2003. Filament formation of MSF-A, a mammalian septin, in human mammary epithelial cells depends on interactions with microtubules. *J. Biol. Chem.* 278:18538–18543.

Rindler, M.J., I.E. Ivanov, and D.D. Sabatini. 1987. Microtubule-acting drugs lead to the nonpolarized delivery of the influenza hemagglutinin to the cell surface of polarized Madin-Darby canine kidney cells. *J. Cell Biol.* 104:231–241.

Rodriguez-Boulan, E., G. Kreitzer, and A. Musch. 2005. Organization of vesicular trafficking in epithelia. *Nat. Rev. Mol. Cell Biol.* 6:233–247.

Spiliotis, E.T., and W.J. Nelson. 2006. Here come the septins: novel polymers that coordinate intracellular functions and organization. *J. Cell Sci.* 119:4–10.

Spiliotis, E.T., M. Kinoshita, and W.J. Nelson. 2005. A mitotic septin scaffold required for Mammalian chromosome congression and segregation. *Science.* 307:1781–1785.

Surka, M.C., C.W. Tsang, and W.S. Trimble. 2002. The mammalian septin MSF localizes with microtubules and is required for completion of cytokinesis. *Mol. Biol. Cell.* 13:3532–3545.

Tagawa, A., A. Mezzacasa, A. Hayer, A. Longatti, L. Pelkmans, and A. Helenius. 2005. Assembly and trafficking of caveolar domains in the cell: caveolae as stable, cargo-triggered, vesicular transporters. *J. Cell Biol.* 170:769–779.

Toomre, D., P. Keller, J. White, J.C. Olivo, and K. Simons. 1999. Dual-color visualization of trans-Golgi network to plasma membrane traffic along microtubules in living cells. *J. Cell Sci.* 112:21–33.

Van der Sluijs, P., M.K. Bennett, C. Antony, K. Simons, and T.E. Kreis. 1990. Binding of exocytic vesicles from MDCK cells to microtubules in vitro. *J. Cell Sci.* 95:545–553.

Wandinger-Ness, A., M.K. Bennett, C. Antony, and K. Simons. 1990. Distinct transport vesicles mediate the delivery of plasma membrane proteins to the apical and basolateral domains of MDCK cells. *J. Cell Biol.* 111:987–1000.

Zhang, J., C. Kong, H. Xie, P.S. McPherson, S. Grinstein, and W.S. Trimble. 1999. Phosphatidylinositol polyphosphate binding to the mammalian septin H5 is modulated by GTP. *Curr. Biol.* 9:1458–1467.